Transport through an impurity tunnel coupled to a Si/SiGe quantum dot

Ryan H. Foote, Daniel R. Ward, J. R. Prance, John King Gamble, Erik Nielsen, Brandur Thorgrimsson, D. E. Savage, A. L. Saraiva, Mark Friesen, S. N. Coppersmith, and M. A. Eriksson

---

Articles you may be interested in

A reconfigurable gate architecture for Si/SiGe quantum dots
Appl. Phys. Lett. **106**, 223507 (2015); 10.1063/1.4922249

Excitation of a Si/SiGe quantum dot using an on-chip microwave antenna
Appl. Phys. Lett. **103**, 132410 (2013); 10.1063/1.4821995

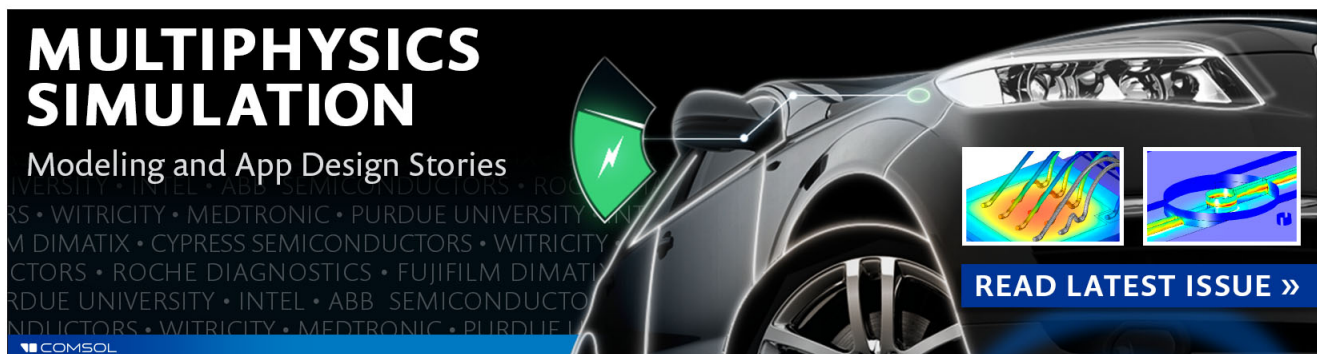Tunable singlet-triplet splitting in a few-electron Si/SiGe quantum dot
Appl. Phys. Lett. **99**, 233108 (2011); 10.1063/1.3666232

Singlet-triplet relaxation in SiGe/Si/SiGe double quantum dots
J. Appl. Phys. **110**, 043716 (2011); 10.1063/1.3625240

Fast tunnel rates in Si/SiGe one-electron single and double quantum dots
Appl. Phys. Lett. **96**, 183104 (2010); 10.1063/1.3425892

Transport through an impurity tunnel coupled to a Si/SiGe quantum dot

Ryan H. Foote,[1,a)] Daniel R. Ward,[1] J. R. Prance,[2] John King Gamble,[3] Erik Nielsen,[3] Brandur Thorgrimsson,[1] D. E. Savage,[1] A. L. Saraiva,[4] Mark Friesen,[1] S. N. Coppersmith,[1] and M. A. Eriksson[1,b)]

[1]Department of Physics, University of Wisconsin-Madison, Madison, Wisconsin 53706, USA
[2]Department of Physics, Lancaster University, Bailrigg, Lancaster LA1 4YB, United Kingdom
[3]Center for Computing Research, Sandia National Laboratories, Albuquerque, New Mexico 87185, USA
[4]Instituto de Física, Universidade Federal do Rio de Janeiro, Caixa Postal 68528, 21941-972 Rio de Janeiro, Brazil

Achieving controllable coupling of dopants in silicon is crucial for operating donor-based qubit devices, but it is difficult because of the small size of donor-bound electron wavefunctions. Here, we report the characterization of a quantum dot coupled to a localized electronic state and present evidence of controllable coupling between the quantum dot and the localized state. A set of measurements of transport through the device enable the determination that the most likely location of the localized state is consistent with a location in the quantum well near the edge of the quantum dot. Our results are consistent with a gate-voltage controllable tunnel coupling, which is an important building block for hybrid donor and gate-defined quantum dot devices. © 2015 AIP Publishing LLC.
[http://dx.doi.org/10.1063/1.4930909]

Donors in silicon are a natural choice for qubits,[1] because their electron and nuclear spins have very long coherence times.[2–7] Although donor-based quantum devices can be fabricated with near-atomically precise placement of donors,[8,9] even when well-placed, it is difficult to control and change the tunnel couplings between them with gate voltages. In contrast, tunnel couplings are easily tunable in gate-defined quantum dots, and high-quality quantum dots hosting at least four different types of spin qubits have been demonstrated.[10–22] Moreover, the electrons in quantum dots can be displaced laterally simply by changing the voltages of the gates on the surface.[23] Because of the differences between donors and quantum dots, it is interesting to ask whether donors or other localized defects can be tunnel-coupled to gate-defined quantum dots in Si/SiGe heterostructures.

Here, we report the observation of a controllable tunnel coupling between a localized electronic state and a gate-defined quantum dot formed in a Si/SiGe heterostructure. We present measurements of transport through the device, demonstrating controllable tunnel coupling between the quantum dot and the localized state. A set of stability diagram measurements enable a determination of the relative magnitude of the capacitance between the surface gates and both the quantum dot and the localized state. We report the expected electron density profiles in the quantum dot and the neighboring reservoirs. Combining the experimental results with 3D capacitive modeling based on the electron density profiles, we determine the most likely location of the localized state in the device. These results demonstrate that it is possible to control the tunnel rate between localized states and quantum dots, notwithstanding the dramatic difference in the characteristic length scales.

A gate-defined quantum dot, shown in Fig. 1, was fabricated in a Si/Si$_{0.68}$Ge$_{0.32}$ heterostructure grown by chemical vapor deposition on a relaxed buffer layer with a surface smoothed by chemical-mechanical polishing. Measurements were performed in a dilution refrigerator with a mixing chamber temperature $T_{MC} < 30$ mK.

Fig. 1(c) shows Coulomb diamonds characteristic of Coulomb blockade with an average charging energy $E_c = 760 \, \mu$eV. By comparing this charging energy with the charging energies of few-electron Si/SiGe quantum dots,[24] we find that this quantum dot is in the many electron regime. We also obtain, from the excited states visible in Fig. 1(c), an estimate of the single-particle energy of about 380 μeV in this quantum dot. The data also enable the extraction of the proportionality constant (the lever arm) $\alpha_{G2} = 148 \, \mu$eV/mV between the voltage on gate G2 and the energy of the quantum dot.

The red arrows near the center of Fig. 1(c) highlight an additional sharp, isolated charging event. Over this range in gate voltage, 13 electrons are added to the main dot, yet only this one additional feature is observed. The capacitances between various gates and the object corresponding to this feature are different from those corresponding to the quantum dot. This difference is made clear in Fig. 1(d), which reports the current through the quantum device as a function of the voltages on gate P and G2. The phenomenology of this plot is very similar to those observed in metal-oxide-semiconductor devices in which donors have been implanted:[25,26] near the center of the scan, a series of shifts in the charge transitions of the dot can be observed; these shifts correspond to the feature marked by the red arrows in Fig. 1(c). The line through the gate voltage space spanned by V_P and V_{G2} connecting these shifts has a different slope than that of the Coulomb blockade peaks corresponding to the dot, confirming the presence of a nearby localized state that is not at the same physical position as the dot. The current at

a)Electronic mail: rhfoote@wisc.edu
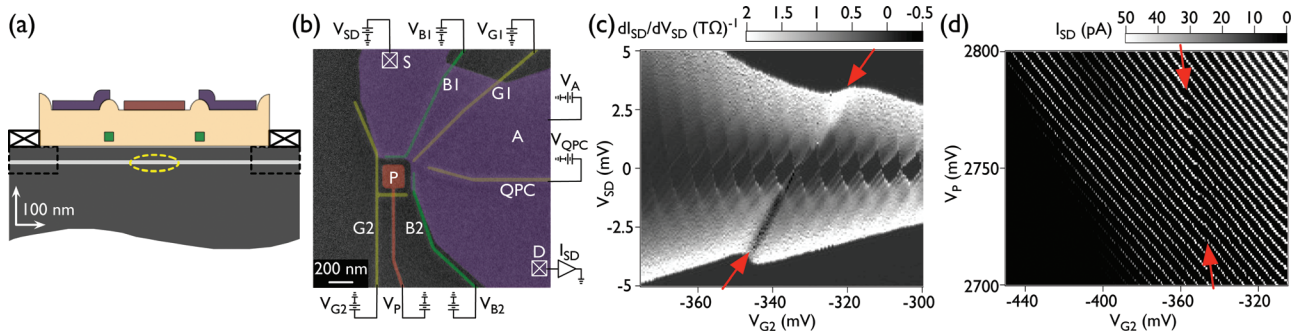b)Electronic mail: maeriksson@wisc.edu

FIG. 1. Device design and characterization. (a) Schematic side view of the device, showing a $Si/Si_{0.68}Ge_{0.32}$ heterostructure with a 10 nm Si well (light grey) and 32 nm SiGe offset (dark grey). Both the upper (purple and red) and lower (green) layers of gates are 2 nm titanium and 20 nm gold deposited by electron beam evaporation. The lower (upper) gates were deposited on 10 nm (90 nm) of atomic layer deposition grown aluminum oxide (light orange). Ohmic contacts S and D (denoted with ⊠ symbols) are 5 nm titanium and 40 nm gold on a region degenerately doped with phosphorus through the quantum well (black dashed boxes). Approximate location of the quantum dot and impurity are shown schematically by the yellow dashed oval. (b) False-color SEM of a device identical to the measured device. Upper gate A (purple) and paddle gate P (red) were positively biased to accumulate a two-dimensional electron gas in the reservoir and to control the energy of the dot, respectively. On the lower level, gates G1, G2, and QPC (yellow) were negatively biased to provide the confinement potential; gates B1 and B2 (green) controlled the tunnel barriers to the source (S) and drain (D) ohmic contacts (denoted with ⊠ symbols). (c) The derivative dI_{SD}/dV_{SD} of the transport current with respect to the gate voltage V_{G2}, showing Coulomb diamonds. A sharp resonance, indicated by arrows, is observed, suggesting a localized state. (d) Coulomb blockade oscillations of the current I_{SD} at fixed $V_{SD} = 100\,\mu V$. The jump indicated by arrows corresponds to the localized state in (c).

the intersection of the charge transitions between the dot and the localized state can be used to gain insight into the tunnel coupling between the localized state and the quantum dot; we show below that this current is a repeatable function of the gate voltages in the device.

Figure 2(a) shows the source-drain current I_{SD} versus V_P and V_{B1}. The dashed black lines indicate the voltages at which the localized state charges, corresponding to the observed shift and gap in the Coulomb blockade peaks. The pattern of lines and slopes in Fig. 2(a) matches the expectation for a two-site system, which here corresponds to the quantum dot and a localized state.[6] No current is observed along the black dashed lines in this figure, indicating that the localized state is not tunnel coupled to both the source and the drain. It is possible, however, that the localized state is connected to either the source or the drain, and this hypothesis is supported by the faintly visible line of current (white in the color scale) that sits at the position of the polarization line at each of the three main intersections in this stability diagram.

Figures 2(b) and 2(c) show a pair of triple points in this two-site system, for two different values of the voltage on gate B2. In both plots, there is no current along the black dashed lines corresponding to the charge transition of the localized site, confirming that the localized site is not tunnel-coupled to both the source and the drain. However, in Fig. 2(b), where $V_{B2} = -402\,mV$, current is observed along the polarization line; in contrast, no such current is observed in Fig. 2(c), where $V_{B2} = -404\,mV$. This current is studied in more detail in Fig. 2(d), where we report line cuts across the polarization line, as indicated by the gray dashed line in Fig. 2(b). Fig. 2(d) shows a dramatic evolution of the current along this path as V_{B2} is changed. For V_{B2} equal to either -398 or $-401\,mV$, no peak in current occurs at the polarization line. In contrast, for intermediate values of $V_{B2} = -399$ and $-400\,mV$, a prominent peak in current is observed at the position of the polarization line. The current peak is visible over a narrow voltage range in V_{B2}. Each line scan in
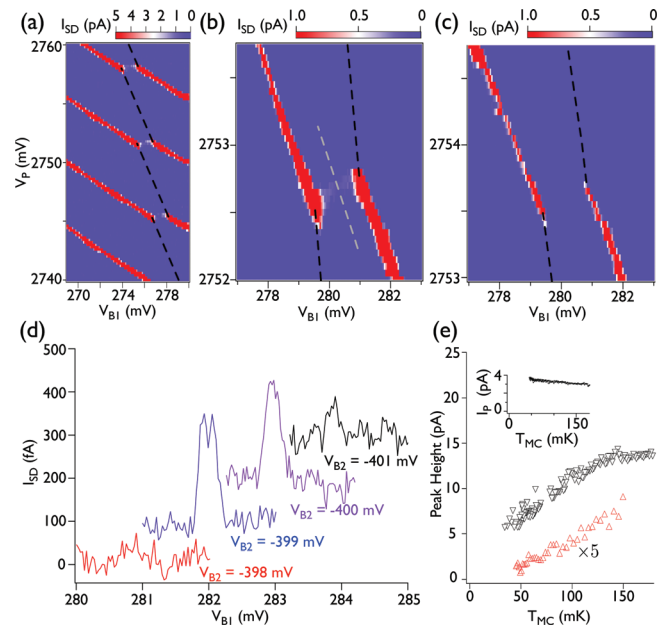

FIG. 2. Control of tunnel coupling. (a) I_{SD} as a function of V_P and V_{B1}, with $V_{B2} = -400\,mV$, showing jumps in the Coulomb blockade transitions. A double dot-like stability diagram is revealed, including a weak polarization line. The localized state charge transitions are not visible and are shown schematically as black dashed lines. (b) and (c) High resolution scans across a polarization line, for $V_{B2} = -402\,mV$ in (b) and $V_{B2} = -404\,mV$ in (c). Current is present at the polarization line in (b) but not in (c). (d) Line scans across the polarization line as a function of V_{B1}, acquired by sweeping V_P and V_{B1} simultaneously, following a path exemplified by the light gray dashed line in panel (b). The data for $V_{B2} = -398\,mV$ are not shifted; subsequent traces are offset vertically by 100 fA and laterally by 1 mV each. These plots, which were acquired in close succession in time, show that changing V_{B2} changes the tunnel couplings to the localized state, turning on and off current at the polarization line. (The overall conditions in this plot are slightly different than those in panels (b) and (c).) (e) Black triangles show the height of the main Coulomb blockade peak near the anticrossing with the localized state, and red triangles show the height of the current peak on the polarization line, both of which are strongly temperature dependent. *Inset:* Coulomb blockade peak height I_P far from the anticrossing with the localized state vs. temperature, showing behavior typical for a large dot at reasonably low temperature.[27]

Fig. 2(d) covers all values of detuning near and at the polarization line, yet only two of them (for specific values of V_{B2}) yield peaks in the measured current. Thus, the tunnel coupling is modified independently of the detuning energy.

The difference between the current peak shown in Fig. 2(d) and the conventional Coulomb peaks corresponding to the quantum dot is also highlighted by the temperature dependence of each peak. The inset to Fig. 2(e) shows the temperature dependence of the Coulomb blockade peak for the single dot, which is tunnel coupled to both the source and the drain, for gate voltages such that the localized state is not involved in the transport. The current is nearly constant as a function of temperature, rising slightly as the temperature drops, consistent with a reasonably large quantum dot at temperatures T for which $kT \ll E_c$ (Ref. 27). In the main panel of Fig. 2(e), the black inverted triangles show the temperature dependence of the main Coulomb blockade peak very close to the anticrossing with the localized state, and the red triangles show the temperature dependence of the current peak on the polarization line. In contrast with the behavior in the inset, both of these peaks increase strongly with increasing temperature. This behavior is consistent with a localized state tunnel coupled to the dot and one (but not both) of the reservoirs. Considering first the main Coulomb peak: on this peak, transport through the dot is allowed (by definition), whereas accessing the localized state requires thermal activation. At elevated temperatures, where transport through the impurity is activated, a significant and new parallel path to exit the dot is opened, increasing the total current by an amount that is comparable to the current in the absence of this new path. Considering the polarization line peak (which is more than 5 times weaker than the main Coulomb peak): this current is suppressed at low temperature. Although charge can shuttle between the dot and the localized state at no energy cost at this position in gate voltage space, it cannot tunnel to or from the leads—raising the temperature activates this process, but only more weakly than for the main Coulomb peak, because additional charge is forbidden on both the dot and the localized state.

To determine the location of the localized state, we combine transport measurements with electrostatic device modeling.[28,29] As shown in Fig. 3(a), we acquire five stability diagrams, sweeping gate voltage V_P, which we use as our reference, as we step five other voltages: V_{G1}, V_{B1}, V_{G2}, V_{QPC}, and V_{B2}. For each scan, all other voltages are held fixed to their values at a central operating point. To interpret these data, we constructed an electrostatic device model in COMSOL Multiphysics,[30] using the device geometry from the experiment, as illustrated in Fig. 3(b). The model was solved in the Thomas-Fermi Approximation,[31,32] with the self-consistent charge accumulation determined using a 2D density of states confined to a sheet at the Si-SiGe interface. We assumed a 2×2 carrier degeneracy due to (2) spin and (2) valley degrees of freedom. The computational domain was $3 \times 5 \, \mu m$ laterally, and included a 100 nm air cap above the oxide layer and 500 nm SiGe substrate below the silicon well. We used zero-field boundary conditions on the sides of the domain and the top of the air cap, and set the conduction band edge to the Fermi level at the bottom of the domain. In addition, we used voltages: $V_{G2} = -0.335 \, V$, $V_{B2} = -0.400 \, V$,
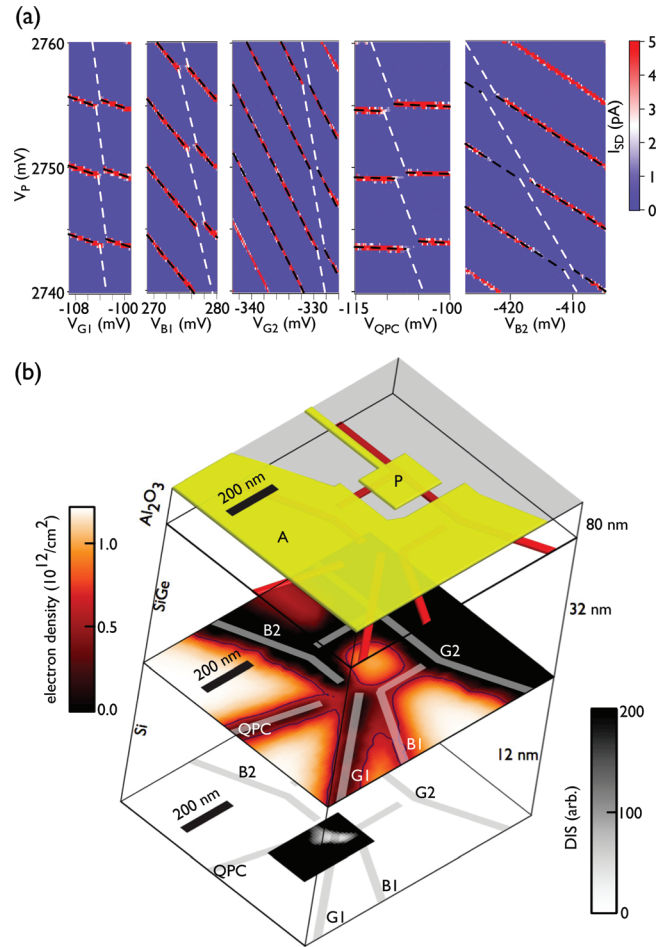

FIG. 3. Locating the localized state by combining experiment and modeling. (a) Stability diagrams at fixed V_{SD} for several gate voltage pairs. The black dashed lines highlight Coulomb blockade transitions of the dot while the white dashed lines show the expected position of the unseen localized state charging event. (b) Results of 3D electrostatic modeling to determine the location of the localized state. The top layer shows the gate geometry of the device local to the dot. The middle layer shows the electron densities of the dot and leads as calculated by COMSOL, with the contour corresponding to 6×10^{11} cm^{-2} electron density. The bottom layer of the device shows the most likely location of the impurity, as determined by the discrepancy metric (Eq. (1)), directly under the tip of gate G1 near the lower Si/SiGe interface about 10 nm below the top of the quantum well.

$V_{QPC} = -0.100 \, V$, $V_{G1} = -0.104 \, V$, $V_{B1} = +0.270 \, V$, $V_A = +2.75 \, V$, and $V_P = +2.75 \, V$.

We approximate the dot and reservoir regions predicted by COMSOL as 5 nm thick metallic sheets at the 6×10^{11} cm^{-2} density contour (Fig. 3(b)), and we treat the localized state as a 1 nm radius metallic sphere. Given a placement of the localized state, we construct a capacitance model predicting each of the experimental stability diagrams.[33] We raster the localized state position across the device and compute as a fit metric a weighted sum-of-squared-differences between experimental and predicted values. We estimate the location of the localized state that is most consistent with the data shown in Fig. 3(a). In particular, we sum the squared differences of (1) the slope of the line connecting all of the "offsets" in the Coulomb blockade lines (the white dashed lines in Fig. 3(b)), and (2) the magnitude of the jump along the y-axis of a Coulomb blockade line due to the localized state. Type 1 quantities are unitless slopes whereas type 2 quantities have units of energy. To combine these into a

single discrepancy metric (DIS), we found empirically that we needed to scale the type 2 quantities reported in meV by 1×10^8 to balance them with the quantities of type 1. Thus, the overall discrepancy metric is

$$DIS = \sum_{i=1}^{5} (PO_i - EO_i)^2 + 1 \times 10^8 \times \sum_{i=1}^{5} (PJ_i - EJ_i)^2, \quad (1)$$

where i indexes each of the five experimental slices shown in Fig. 3(a), PO and EO are the predicted and experimental type 1 offset quantities, and PJ and EJ are the predicted and experimental type 2 jump quantities respectively. The lower layer of Fig. 3(b) shows a cut of DIS along a plane 12 nm beneath the top of the strained Si well, identifying a region under the tip of gate G1 as the most likely region in the x-y plane to find the localized state. The DIS value is not very sensitive to the depth (z-coordinate) between 10 and 20 nm; the 12 nm data are shown.

We propose a tunnel rate dependent model of our hybrid quantum dot-impurity system. Under typical device operation, the impurity is tunnel coupled to one of the leads and only very weakly tunnel-coupled to the dot. Under these conditions, a charging event of the localized state varies the electric field local to the dot, changing the Coulomb blockade condition and resulting in the familiar jump in the dot charge transition from Fig. 2(c). Changing the voltage of the tunnel barrier V_{B2} changes the dot-drain, impurity-drain, and dot-impurity tunnel rates. While the exact dependence on V_{B2} of each of these tunnel rates is complicated and difficult to predict, for certain gate voltage tunings, like those shown in Fig. 2(b), the dot-impurity tunnel rate increases, and the three tunnel rates together—especially the enhanced dot-impurity tunnel rate—allow for current through the normally blockaded region as well as enhancement of current corresponding to the dot charge transitions.

In conclusion, we have shown measurements and modeling of a tunnel-coupled quantum dot-impurity system in a Si/SiGe heterostructure. We demonstrated tunable tunnel coupling between the impurity and the dot that is controlled by varying a nearby gate voltage, and we reported the temperature dependence of the coupled system. We also have found the most likely position of the localized state through capacitive modeling, with the capacitances extracted from this model in good agreement with the experimental results. Moving forward, we propose that the use of quantum wells closer to the surface and gate electrodes placed more closely together should enable even finer control over the coupling between a localized state and a quantum dot.

[1]B. E. Kane, Nature **393**, 133 (1998).
[2]J. J. L. Morton, A. M. Tyryshkin, R. M. Brown, S. Shankar, B. W. Lovett, A. Ardavan, T. Schenkel, E. E. Haller, J. W. Ager, and S. A. Lyon, Nature **455**, 1085 (2008).
[3]D. R. McCamey, J. Van Tol, G. W. Morley, and C. Boehme, Science **330**, 1652 (2010).
[4]J. J. Pla, K. Y. Tan, J. P. Dehollain, W. H. Lim, J. J. L. Morton, D. N. Jamieson, A. S. Dzurak, and A. Morello, Nature **489**, 541 (2012).
[5]A. M. Tyryshkin, S. Tojo, J. J. L. Morton, H. Riemann, N. V. Abrosimov, P. Becker, H.-J. Pohl, T. Schenkel, M. L. W. Thewalt, K. M. Itoh, and S. A. Lyon, Nat. Mater. **11**, 143 (2012).
[6]F. A. Zwanenburg, A. S. Dzurak, A. Morello, M. Y. Simmons, L. C. L. Hollenberg, G. Klimeck, S. Rogge, S. N. Coppersmith, and M. A. Eriksson, Rev. Mod. Phys. **85**, 961 (2013).
[7]J. T. Muhonen, J. P. Dehollain, A. Laucht, F. E. Hudson, R. Kalra, T. Sekiguchi, K. M. Itoh, D. N. Jamieson, J. C. McCallum, A. S. Dzurak, and A. Morello, Nat. Nanotechnol. **9**, 986 (2014).
[8]S. Schofield, N. Curson, M. Simmons, F. Rueß, T. Hallam, L. Oberbeck, and R. Clark, Phys. Rev. Lett. **91**, 136104 (2003).
[9]M. Fuechsle, S. Mahapatra, F. A. Zwanenburg, M. Friesen, M. A. Eriksson, and M. Y. Simmons, Nat. Nanotechnol. **5**, 502 (2010).
[10]J. R. Petta, A. C. Johnson, J. M. Taylor, E. A. Laird, A. Yacoby, M. D. Lukin, C. M. Marcus, M. P. Hanson, and A. C. Gossard, Science **309**, 2180 (2005).
[11]M. Pioro-Ladrière, T. Obata, Y. Tokura, Y.-S. Shin, T. Kubo, K. Yoshida, T. Taniyama, and S. Tarucha, Nat. Phys. **4**, 776 (2008).
[12]L. Gaudreau, G. Granger, A. Kam, G. C. Aers, S. A. Studenikin, P. Zawadzki, M. Pioro-Ladrière, Z. R. Wasilewski, and A. S. Sachrajda, Nat. Phys. **8**, 54 (2011).
[13]K. Nowack, M. Shafiei, M. Laforest, G. Prawiroatmodjo, L. Schreiber, C. Reichl, W. Wegscheider, and L. Vandersypen, Science **333**, 1269 (2011).
[14]B. M. Maune, M. G. Borselli, B. Huang, T. D. Ladd, P. W. Deelman, K. S. Holabird, A. A. Kiselev, I. Alvarado-Rodriguez, R. S. Ross, A. E. Schmitz, M. Sokolich, C. A. Watson, M. F. Gyure, and A. T. Hunter, Nature **481**, 344 (2012).
[15]K. D. Petersson, L. W. McFaul, M. D. Schroer, M. Jung, J. M. Taylor, A. A. Houck, and J. R. Petta, Nature **490**, 380 (2012).
[16]M. D. Shulman, O. E. Dial, S. P. Harvey, H. Bluhm, V. Umansky, and A. Yacoby, Science **336**, 202 (2012).
[17]J. R. Prance, Z. Shi, C. B. Simmons, D. E. Savage, M. G. Lagally, L. R. Schreiber, L. M. K. Vandersypen, M. Friesen, R. Joynt, S. N. Coppersmith, and M. A. Eriksson, Phys. Rev. Lett. **108**, 046808 (2012).
[18]J. Medford, J. Beil, J. M. Taylor, S. D. Bartlett, A. C. Doherty, E. I. Rashba, D. P. DiVincenzo, H. Lu, A. C. Gossard, and C. M. Marcus, Nat. Nanotechnol. **8**, 654 (2013).
[19]E. Kawakami, P. Scarlino, D. R. Ward, F. R. Braakman, D. E. Savage, M. G. Lagally, M. Friesen, S. N. Coppersmith, M. A. Eriksson, and L. M. K. Vandersypen, Nat. Nanotechnol. **9**, 666 (2014).
[20]D. Kim, Z. Shi, C. B. Simmons, D. R. Ward, J. R. Prance, T. S. Koh, J. K. Gamble, D. E. Savage, M. G. Lagally, M. Friesen, S. N. Coppersmith, and M. A. Eriksson, Nature **511**, 70 (2014).
[21]Z. Shi, C. B. Simmons, D. R. Ward, J. R. Prance, X. Wu, T. S. Koh, J. K. Gamble, D. E. Savage, M. G. Lagally, M. Friesen, S. N. Coppersmith, and M. A. Eriksson, Nat. Commun. **5**, 3020 (2014).
[22]M. Veldhorst, J. C. C. Hwang, C. H. Yang, A. W. Leenstra, B. de Ronde, J. P. Dehollain, J. T. Muhonen, F. E. Hudson, K. M. Itoh, A. Morello, and A. S. Dzurak, Nat. Nanotechnol. **9**, 981 (2014).
[23]Z. Shi, C. B. Simmons, J. Prance, J. K. Gamble, M. Friesen, D. E. Savage, M. G. Lagally, S. N. Coppersmith, and M. A. Eriksson, Appl. Phys. Lett. **99**, 233108 (2011).
[24]C. B. Simmons, M. Thalakulam, N. Shaji, L. J. Klein, H. Qin, R. H. Blick, D. E. Savage, M. G. Lagally, S. N. Coppersmith, and M. A. Eriksson, Appl. Phys. Lett. **91**, 213103 (2007).
[25]A. Morello, J. Pla, F. Zwanenburg, K. Chan, K. Tan, H. Huebl, M. Mottonen, C. Nugroho, C. Yang, J. van Donkelaar, A. Alves, D. Jamieson, C. Escott, L. Hollenberg, R. Clark, and A. Dzurak, Nature **467**, 687 (2010).

[26]M. Urdampilleta, A. Chatterjee, C. C. Lo, T. Kobayashi, S. Barraud, A. C. Betz, S. Rogge, M. F. Gonzalez-Zalba, and J. J. L. Morton, Phys. Rev. X **5**, 031024 (2015).

[27]H. van Houten, C. W. J. Beenakker, and A. A. M. Staring, "Coulomb-blockade oscillations in semiconductor nanostructures," in *Single Charge Tunneling*, edited by H. Grabert and M. H. Devoret (Plenum, New York, 1992).

[28]N. C. Bishop, R. W. Young, G. A. TenEyck, J. R. Wend, E. S. Bielejec, K. Eng, L. A. Tracy, M. P. Lilly, M. S. Carroll, C. B. Pinilla, and H. L. Stalford, "Triangulating the source of tunneling resonances in a point contact with nanometer scale sensitivity," presented at APS March Meeting 2011, Dallas, TX, 21–25 March 2011; preprint arXiv:1107.5104 (2011).

[29]F. A. Mohiyaddin, R. Rahman, R. Kalra, G. Klimeck, L. C. L. Hollenberg, J. J. Pla, A. S. Dzurak, and A. Morello, Nano Lett. **13**, 1903 (2013).

[30]See http://www.comsol.com for information about the COMSOL software package.

[31]M. Stopa, Phys. Rev. B **54**, 13767 (1996).

[32]A. R. Schmidt, E. Henry, C. C. Lo, Y.-T. Wang, H. Li, L. Greenman, O. Namaan, T. Schenkel, K. B. Whaley, J. Bokor, E. Yablonovitch, and I. Siddiqi, J. Appl. Phys. **116**, 044503 (2014).

[33]W. G. Van Der Wiel, T. Fujisawa, S. Tarucha, and L. P. Kouwenhoven, Rev. Mod. Phys. **75**, 1 (2003).